ACS APPLIED MATERIALS & INTERFACES

www.acsami.org

Research Article

Quasi-Liquid Surfaces for Sustainable High-Performance Steam Condensation

Deepak Monga, Zongqi Guo, Li Shan, Seyed Adib Taba, Jyotirmoy Sarma, and Xianming Dai*

Cite This: *ACS Appl. Mater. Interfaces* 2022, 14, 13932−13941

Read Online

ACCESS | Metrics & More | Article Recommendations | Supporting Information

ABSTRACT: Sustainable high-performance steam condensation is critical to reducing the size, weight, and cost of water and energy systems. It is well-known that dropwise condensation can provide a significantly higher heat-transfer coefficient than filmwise condensation. Tremendous efforts have been spent to promote dropwise condensation by achieving a nonwetting state on superhydrophobic surfaces and a slippery state on liquid-infused surfaces, but these surfaces suffer from severe durability challenges. Here, we report sustainable high-performance dropwise condensation of steam on newly developed durable quasi-liquid surfaces, which are easily made by chemically bonding quasi-liquid polymer molecules on solid substrates. As a result, the solid/water interface is changed to a quasi-liquid/water interface with minimal adhesion and extraordinary durability. The quasi-liquid surface with ultralow contact angle hysteresis down to 1° showed a heat-transfer coefficient up to 70 and 380% higher than those on conventional hydrophobic and hydrophilic surfaces, respectively. Furthermore, we demonstrated that the quasi-liquid coating exhibited a sustainable heat-transfer coefficient of 71 kW/(m^2 K) at a heat flux of 420 kW/m^2 under a prolonged period of 39 h in continuous steam condensation. Such a quasi-liquid surface has the potential to sustain high-performance dropwise condensation of steam and address the long-standing durability challenge in the field.

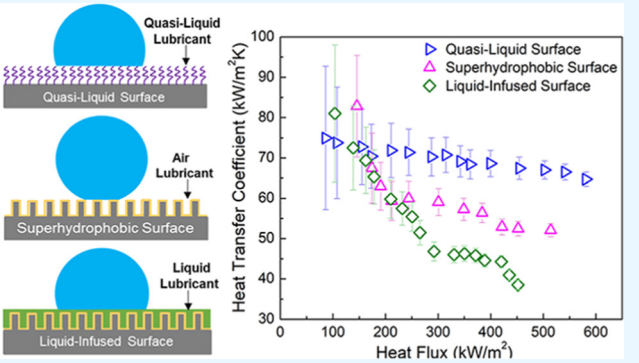

KEYWORDS: *steam condensation, heat transfer, quasi-liquid surface, contact angle hysteresis, durability*

INTRODUCTION

Condensation of steam plays a significant role in thermal energy systems, including power generation, desalination, water harvesting, and thermal management.[1−4] Industrial condensers typically show a filmwise condensation due to their hydrophilic surfaces. In filmwise condensation, condensed fluids spread over the surface and form a thick condensate layer that provides a large thermal resistance. However, dropwise condensation with discrete liquid droplets provides an order of magnitude higher heat-transfer performance than filmwise condensation.[1] Therefore, both active and passive ways were reported to enhance dropwise condensation. Active ways include the use of electric fields and vibration-assisted droplet departure, but they need external energy.[5−7] Passive ways to promote dropwise condensation on flat solid hydrophobic surfaces include organic films,[8,9] monolayer coatings,[10] ion implantation,[11,12] polymer films,[13] and graphene coating.[14] Although these flat surfaces enhanced heat-transfer performances, they showed a large contact angle hysteresis (CAH) above 5°, resulting in slow condensate removal.[10,13,14] Superhydrophobic surfaces (SHS) with a contact angle (CA) above 150° and a contact angle hysteresis below 5° use micro/nanoscale structures with air as a lubricant to further promote condensate removal.[15−17] When droplets partially floated on the air gaps of SHS, coalescence-induced jumping droplets were observed.[15,18] However, at an elevated subcooling, nanoscale droplets nucleate within the surface textures, and transition occurs from the jumping to flooding.[15,19] Significant efforts have been spent to delay the dropwise-to-filmwise transition such as the three-dimensional (3D) nanowire networks without microcracks[17] and patterned superhydrophobic surfaces with wettability contrast.[20−24] These surfaces could enhance condensation and delay flooding, but they still rely on air gaps, which could not prevent the dropwise-to-filmwise transition.

To resolve the challenges of air displacement on superhydrophobic surfaces, researchers created slippery liquid-infused porous surfaces (SLIPS) or liquid-infused surfaces.[25,26] SLIPS shows more stable droplet removal capabilities due to the transition from air to liquid lubrication. These provide a low CAH $\Delta\theta$, where $\Delta\theta = \theta_{adv} - \theta_{rec}$, θ_{adv} is the advancing

Received: January 7, 2022
Accepted: March 7, 2022
Published: March 15, 2022

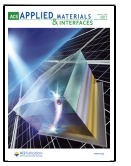

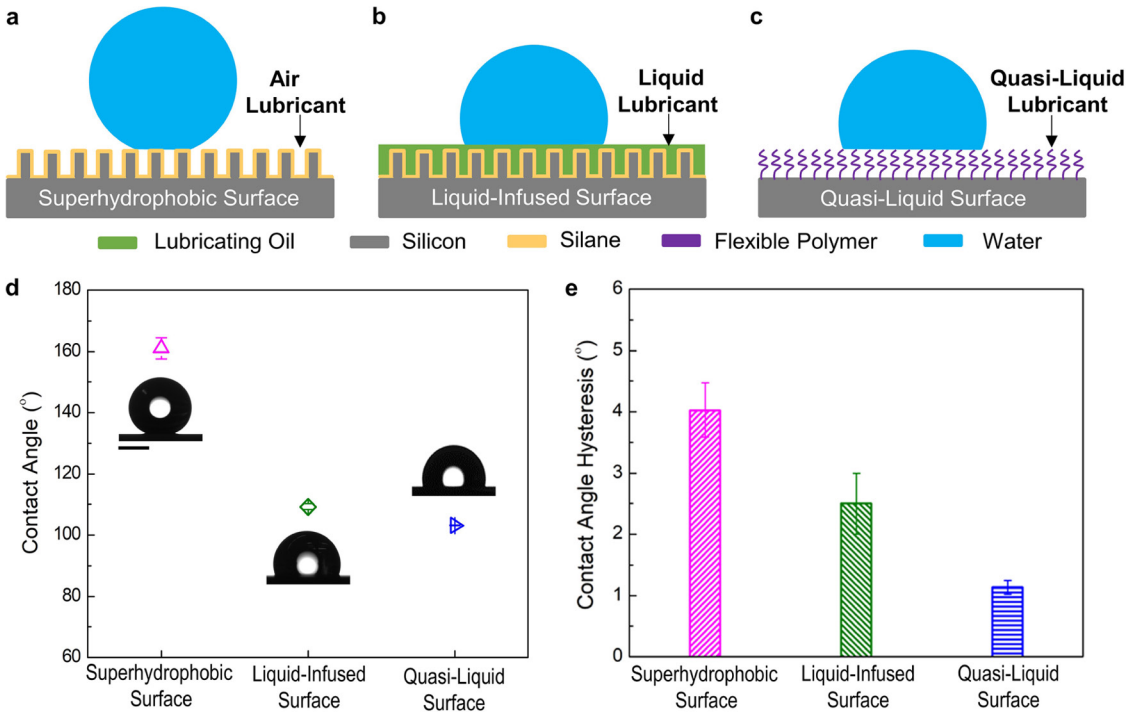

Figure 1. Quasi-liquid surfaces addressed the durability challenges of air and liquid lubricated surfaces. Schematic of a water droplet on (a) superhydrophobic surface, (b) liquid-infused surface, and (c) quasi-liquid surface. (d) Contact angle (CA) and (e) contact angle hysteresis (CAH) on the superhydrophobic surface, liquid-infused surface, and quasi-liquid surface. The scale bar is 1 mm.

contact angle and θ_{rec} is the receding contact angle.[16,27−29] Hydrophobic SLIPS with a hydrophobic liquid lubricant showed high droplet removal capabilities but suffered from poor droplet nucleation density.[16,27] Hydrophilic SLIPS showed the meniscus-mediated coarsening effect,[30] and hydrophilic slippery rough surfaces demonstrated promising droplet mobility due to the small CAH and large surface areas.[31] However, all liquid-infused surfaces suffer from lubricant depletion due to the inevitable wrapping layer (also called cloaking). As a result, the heat-transfer performance degrades over time.[32,33] Brushed lubricant-impregnated surfaces demonstrated the use of a brush to replenish the depleted oil for long-term operation and improved heat transfer. However, this active approach requires physical contact with the rotational tube and majorly the removal of droplets by the contact of the brush with the condensing surface.[34] Polymer-infused porous surfaces (PIPS) reported a reduced thermal resistance by infusing polymer into porous nanostructures and enhanced heat-transfer coefficient.[35] The heat-transfer coefficient on PIPS was increased by 6−8 folds compared to that of filmwise condensation. The heat-transfer enhancement on the PIPS is comparable to that on iCVD surfaces,[35] which is 7 times higher than that of filmwise condensation.[13] Nonetheless, nanowire PIPS showed a high CAH of 16°. The durability challenges impede the potential applications of superhydrophobic surfaces and liquid-infused surfaces even though they are able to enhance condensation heat transfer. Recently, researchers developed the surfaces with grafted flexible polymer chains on flat surfaces to form a liquid-like layer, which showed excellent oil repellency, self-cleaning, and antifouling.[36−38] However, the application for steam condensation is not reported yet.

Here, we report sustainable high-performance dropwise condensation of steam on a durable quasi-liquid surface (QLS) that can potentially overcome the durability challenges of superhydrophobic surfaces and liquid-infused surfaces. Such a super slippery and durable surface was made by tethering one end of the flexible polymer on solid substrates while keeping the other end mobile. The quasi-liquid surface showed a contact angle of 105° with tunable contact angle hysteresis. The QLS that was made from vapor-phase grafting showed an ultralow CAH down to 1°.[39] It demonstrated a high droplet departure speed with heat-transfer enhancement up to 70% compared to silane coating. The quasi-liquid surface exhibits a sustainable high heat-transfer coefficient of 71 kW/(m^2 K) for a prolonged period of 39 h at the heat flux of 420 kW/m^2 under day-and-night steam condensation.

RESULTS AND DISCUSSION

Quasi-Liquid Surface: Address the Durability Challenge of Air and Liquid Lubricated Surfaces. To investigate the heat-transfer performance of QLS under pure steam condensation without noncondensable gases, the experiments were conducted in a closed chamber with a steam pressure of 6.9 kPa above atmospheric pressure. The quasi-liquid surface was fabricated using vapor-phase grafting (see the Methods section for details). SHS and SLIPS were selected as control studies for two reasons: (i) SHS has been well studied in jumping droplet condensation and showed a high heat-transfer performance;[15,17] (ii) SLIPS has enhanced heat transfer with high droplet mobility due to liquid lubrication.[25,32] SHS with a high apparent CA of 160 ± 3.5° and CAH of 4 ± 0.5° allow droplets to achieve a Cassie wetting state with air gaps underneath (Figure 1a), while SLIPS is made by infusing a liquid lubricant within the textured surface, which has a homogeneous and smooth liquid−liquid interface (Figure 1b). Mineral oil was used as a lubricant for the fabrication of SLIPS because it could

https://doi.org/10.1021/acsami.2c00401
ACS Appl. Mater. Interfaces 2022, 14, 13932−13941

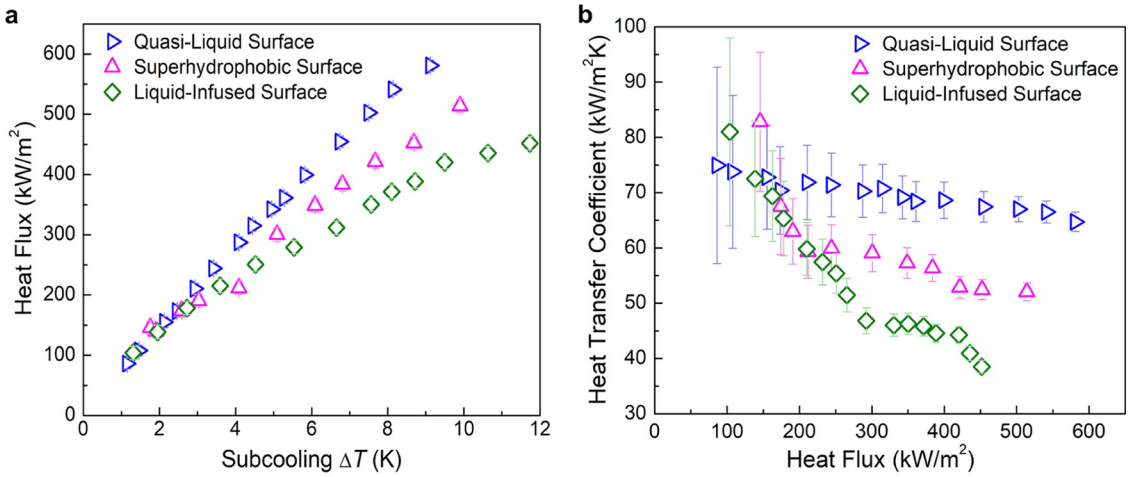

Figure 2. Heat-transfer performance of steam condensation on the quasi-liquid surface. (a) Experimental heat flux with different subcooling and (b) experimental heat-transfer coefficient as a function of heat flux on SHS, SLIPS, and QLS.

minimize the wrapping layer[40] and showed excellent performance for water harvesting.[41] In this work, we developed a durable quasi-liquid surface by tethering one end of the mobile polymer molecules (i.e., liquid poly(dimethylsiloxane) (PDMS)) but keeping the other end mobile (Figure 1c). QLS behaves like a liquid layer due to highly mobile molecule chains on the untethered end,[39] resulting in an ultralow CAH. A goniometer was used to measure the CAH on SHS, SLIPS, and QLS (Figure 1d). QLS has an ultralow CAH of 1 ± 0.1°, while SHS ($\Delta\theta$ = 4°) and SLIPS ($\Delta\theta$ = 2.5°) have relatively higher CAH (Figure 1e).

We experimentally compared the heat-transfer performance on QLS with those on SHS and SLIPS. The heat flux increases with the increase of subcooling on the tested three surfaces (Figure 2a). SHS and SLIPS show a heat-transfer coefficient above 81 kW/(m^2 K) at the low heat flux ($q'' \leq$ 165 kW/m^2) (Figure 2b). With the increase of heat flux, the heat-transfer performances decrease on SHS and SLIPS. However, QLS demonstrates sustainable heat-transfer performance from low heat flux to high heat flux. It shows a higher heat-transfer coefficient of 71 kW/(m^2 K) at the heat flux of 420 kW/m^2, which is 30 and 60% higher than that on SHS and SLIPS at the same heat flux, respectively. The high heat-transfer coefficient on SHS at low heat flux is due to coalescence-induced droplet jumping.[15] Due to spontaneous jumping, a large number of small droplets leave the surface. The refreshed area can condense more water droplets. However, with the increase of heat flux, the condensation mode transitions from jumping to partial wetting with droplets sliding (Movie S1). At an elevated heat flux, the nucleation size decreases due to reduced nucleation energy barrier, and nanoscale droplets nucleate within the gaps of the surface structures (Figure S1).[17] This reduces the droplet mobility and heat-transfer coefficient. Meanwhile, SLIPS shows a high heat-transfer coefficient at a low heat flux due to the high droplet mobility. The liquid lubricant provides a fast droplet shedding with a small departure diameter (Figure S2). However, the liquid lubricant depletes over time due to the wrapping layer on shedding droplets.[42] Due to lubricant depletion on SLIPS, the droplet mobility decreases, and the droplet departure size increases (Movie S1), leading to the decrease of the heat-transfer coefficient. The sustained heat-transfer coefficient on QLS is attributed to its slippery interface, which enhances droplet mobility and shedding at a smaller diameter due to the ultralow CAH (Movies S1). Meanwhile, QLS shows a stable dropwise condensation over the wide range of heat flux (10−600 kW/m^2), while SHS and SLIPS could only show superior dropwise condensation at a low heat flux.

We further analyzed the departure frequency (i.e., the number of droplets that depart from the surface per second) to quantitatively understand the heat transfer. QLS shows a departure frequency of 270 droplets/s at a subcooling of 6 K, which is 125 and 145% higher than those on SHS and SLIPS, respectively (Figure S3 and Movie S1). The higher departure frequency on QLS due to its ultralow CAH leads to a higher heat-transfer coefficient. However, the partial wetting on SHS and lubricant depletion on SLIPS lead to reduced departure frequencies and heat-transfer performances. Even though the SHS and SLIPS showed enhanced condensation, the durability challenges restrict the potential application of both surfaces. Thus, we demonstrated that the durable QLS can achieve a stable dropwise condensation at a broad range of heat fluxes. Furthermore, we demonstrated dropwise condensation on the QLS-coated aluminum using vapor-phase grafting (Figure S4 and Section S3). QLS-coated aluminum shows a CAH of 4°. However, silane-coated aluminum has a CAH of 11° and the coating failed under continuous steam condensation, probably due to the large pinning forces and weak bonding of the silane coating on aluminum substrates. The mechanism for the large pinning force and weak bonding is the cross-linking of silane molecules, leading to the formation of agglomerates on the surface.[43] Previous work shows that the silane coating is not robust and degrades within a minute in steam condensation.[13] QLS-coated aluminum shows a heat-transfer coefficient of 45 kW/(m^2 K) (Section S3), while the QLS-coated silicon has a heat-transfer coefficient of 71 kW/(m^2 K) at the heat flux of 420 kW/m^2. The higher heat transfer on QLS-coated silicon is attributed to the low CAH ($\Delta\theta$ = 1°), leading to a higher droplet mobility than that on QLS-coated aluminum ($\Delta\theta$ = 4°).

Ultralow Contact Angle Hysteresis for Heat-Transfer Enhancement. A low contact angle hysteresis is desirable to enhance the heat-transfer coefficient.[44] Thus, we further investigated the role of ultralow contact angle hysteresis on QLS by comparing the surfaces with different CAH but identical CA. Two different fabrication methods, the vapor-

https://doi.org/10.1021/acsami.2c00401
ACS Appl. Mater. Interfaces 2022, 14, 13932−13941

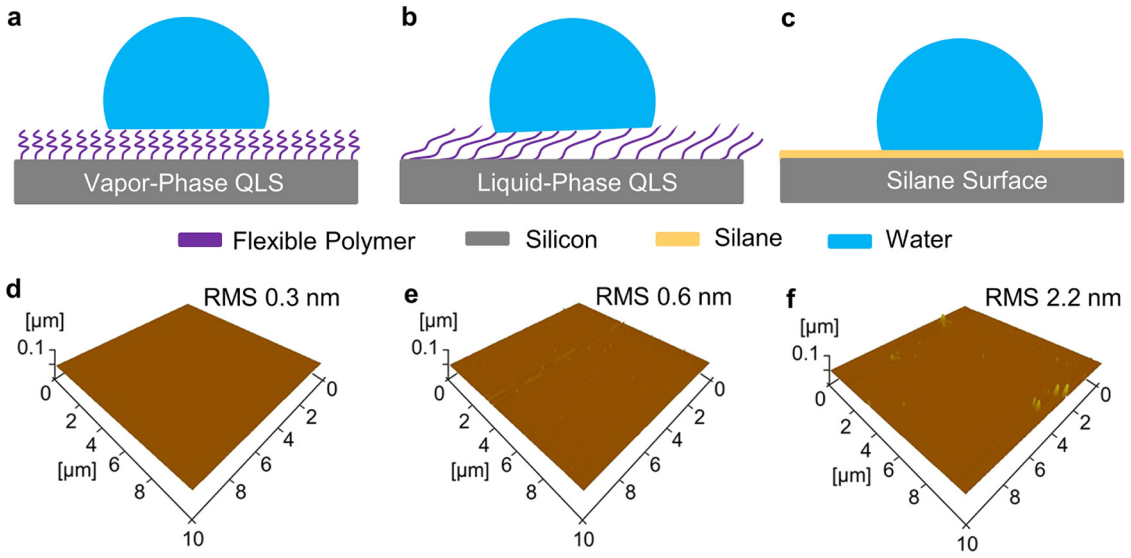

Figure 3. Schematic of a water droplet on (a) vapor-phase QLS, (b) liquid-phase QLS, and (c) silane surface. 3D AFM images of (d) vapor-phase QLS, (e) liquid-phase QLS, and (f) silane surface.

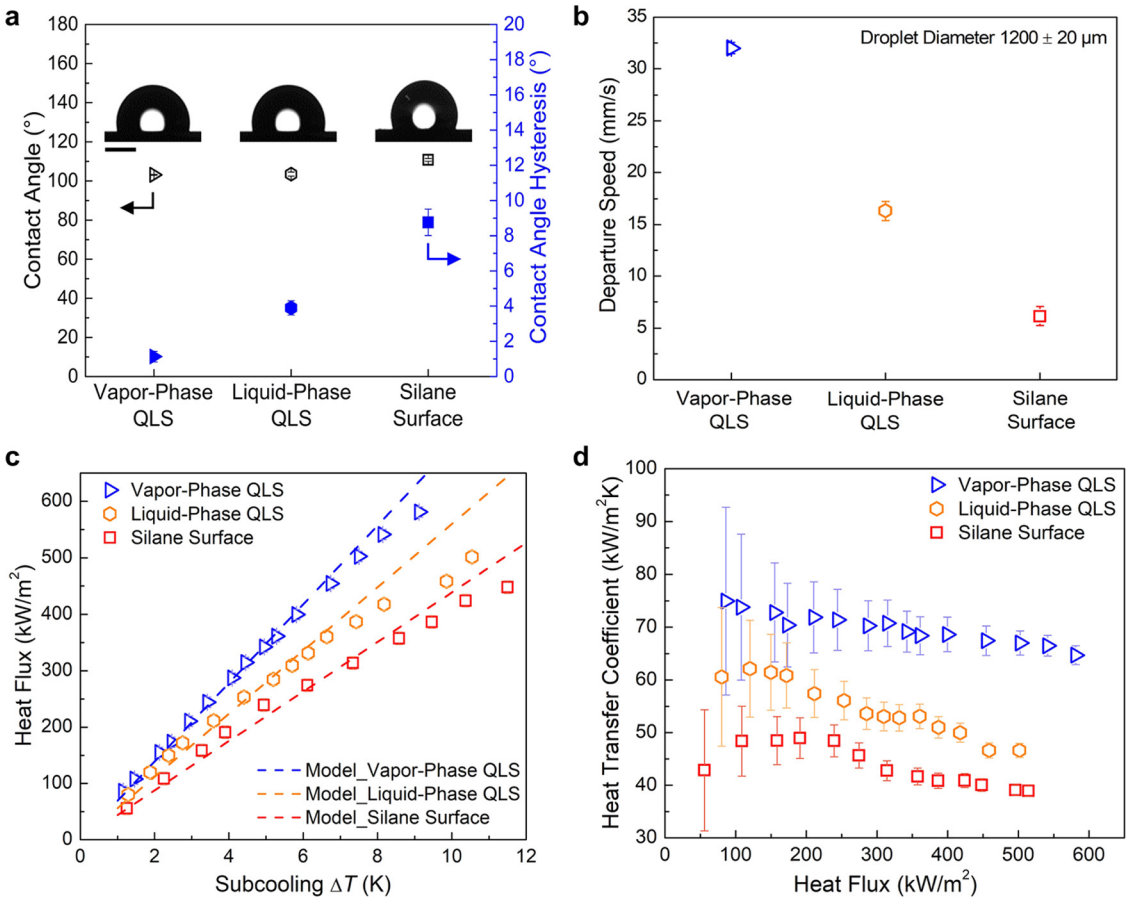

Figure 4. Ultralow contact angle hysteresis promotes heat transfer when the contact angle is nearly identical. (a) CA and CAH on three surfaces. The scale bar is 1 mm. (b) Departure speed on three surfaces at the subcooling of 9 K. (c) Experimental and theoretical heat flux as a function of subcooling. (d) Experimental heat-transfer coefficient as a function of heat flux.

phase (Figure 3a) and the liquid-phase grafting (Figure 3b), are used to make the QLS. The chlorine-terminated PDMS with molecular weight (MW) of 4000 g/mol was used for the vapor-phase grafting, while trimethylsiloxy-terminated PDMS (i.e., silicone oil) with a molecular weight of 17 250 g/mol was used for the liquid-phase grafting (Figure S5). The silane surface was used as a control surface because silane coating has been well studied for dropwise condensation (Figure 3c).[13] Vapor-phase QLS with a low molecular weight has short chains perpendicular to the surface. These short chains are highly

https://doi.org/10.1021/acsami.2c00401
ACS Appl. Mater. Interfaces 2022, 14, 13932−13941

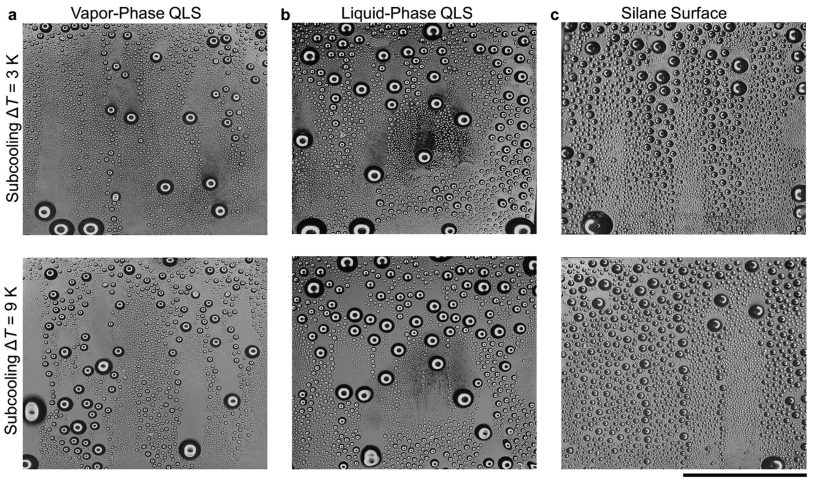

Figure 5. Rapid condensate removal on the quasi-liquid surface. Dropwise condensation with shedding droplets on (a) vapor-phase QLS, (b) liquid-phase QLS, and (c) silane surface at the subcooling of 3 and 9 K. The scale bar is 1 cm.

flexible due to nonentanglement.[45] The atomic force microscope (AFM) images showed that the vapor-phase QLS has an extremely smooth surface due to molecular chains with high flexibility and grafting uniformity (Figure 3d). However, the liquid-phase QLS with a high molecular weight has elongated chains that orient parallel to the surface. The liquid-phase QLS might have entanglement between adjacent polymer molecules, resulting in a slightly higher roughness (Figure 3e) and the silane surface has a larger roughness due to the rigid molecular chains (Figure 3f).[46] Vapor-phase QLS has an ultralow CAH ($\Delta\theta$ = 1°), which is much lower than liquid-phase QLS ($\Delta\theta$ = 3.5°) and silane surface ($\Delta\theta$ = 9.0°) (Figure 4a). The vapor-phase QLS shows an ultralow CAH due to highly flexible molecular chains without entanglement, while the liquid-phase QLS has a higher CAH due to the entanglement of elongated molecular chains and increases the CAH. The droplet departure diameters on vapor-phase QLS, liquid-phase QLS, and silane surface are 380, 600, and 1150 μm, respectively. Therefore, the droplet diameter of 1200 ± 20 μm was selected to compare the departure speed on these surfaces (Figure 4b).

We further compared the heat-transfer performances and measured the droplet departure speeds on these surfaces with varying CAH. Vapor-phase QLS shows a heat flux of 580 kW/m^2, while liquid-phase QLS and silane surface have a heat flux of 460 and 420 kW/m^2 at a subcooling of 9 K (Figure 4c). The high droplet mobility with low adhesion and droplet shedding at a smaller diameter on vapor-phase QLS significantly reduce the thermal resistance of condensate droplets, which leads to a high heat-transfer performance. Vapor-phase QLS has approximately 200 and 600% higher droplet departure speed than liquid-phase QLS and silane surfaces. The high departure speed on vapor-phase QLS is attributed to higher droplet mobility due to ultralow CAH owing to its highly flexible molecular chains.[39] However, the liquid-phase QLS and silane surface have reduced droplet mobility and departure speed due to relatively higher CAH (Movies S2 and S3), resulting in lower heat-transfer performances on liquid-phase QLS and the silane surface.

To further understand the influence of CAH, we compared the experimental heat-transfer performance (Section S4 and Figures S6 and S7) with a theoretical dropwise condensation model for validation on three surfaces: vapor-phase QLS, liquid-phase QLS, and silane surface. The theoretical heat flux was calculated by integrating the heat transfer through individual droplets (Figure S8) with droplet number density (see Section S6 for details). The theoretical heat flux shows a good agreement with the experimental heat flux and the dropwise condensation model could predict the experimental results (Figure 4c). The experimental heat-transfer coefficient of 71 kW/(m^2 K) at the heat flux of 420 kW/m^2 on vapor-phase QLS shows a heat-transfer enhancement of 40 and 70% compared to the liquid-phase QLS and silane surface, respectively (Figure 4d). It could also increase the heat-transfer coefficient by approximately 380% compared with the hydrophilic silicon surface (Figure S7). This shows that the ultralow CAH on vapor-phase QLS provides a rapid condensate removal, which could reduce the thermal resistance of the condensate and leads to a heat-transfer enhancement.

Rapid Condensate Removal on the Quasi-Liquid Surface. To elucidate the effect of ultralow contact angle hysteresis on the condensate removal through droplet departure, we investigated the condensation modes and droplet dynamics on three flat surfaces: vapor-phase QLS, liquid-phase QLS, and silane surface. Droplet behaviors were visualized on the vertically mounted condensing surfaces (Figure S6 and Section S4 for details). Vapor-phase QLS shows continual droplet growth and sliding at elevated subcooling (Figure 5a). Due to the ultralow CAH, condensed droplets are highly mobile on the vapor-phase QLS and depart rapidly from the surface (Movie S2). With an increased subcooling, the droplet departure frequency further increases without flooding (Movie S3). Liquid-phase QLS exhibits slower droplet mobility and larger droplet departure diameter with large size droplets due to a higher CAH than that on the vapor-phase QLS (Figure 5b and Movies S2 and S3). The silane surface shows a conventional dropwise condensation where the droplet departs when the gravity overcomes the contact line pinning force (Figure 5c). The droplet removal frequency on vapor-phase QLS is 27 Hz, while the liquid-phase QLS and silane surface show approximately 50 and 19% droplet removal frequencies compared to that on vapor-phase QLS, respectively, at the subcooling of 9 K (Figure S9). Due to the ultralow CAH, the condensed droplets show small pinning forces with rapid droplet removal.

https://doi.org/10.1021/acsami.2c00401
ACS Appl. Mater. Interfaces 2022, 14, 13932−13941

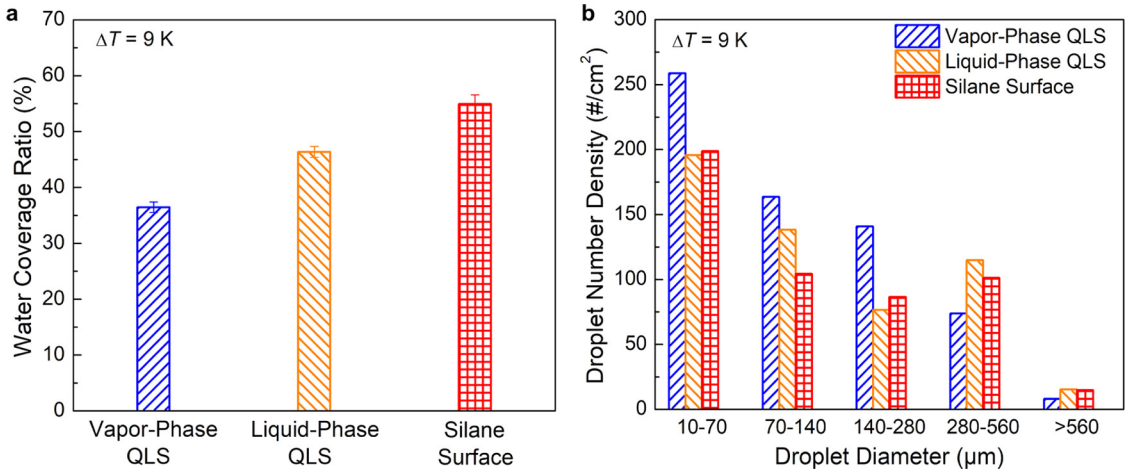

Figure 6. Droplet dynamics on vapor-phase QLS, liquid-phase QLS, and silane surface. (a) Water coverage ratio and (b) droplet number density at a subcooling of 9 K.

Table 1. Various Quasi-Liquid Surfaces for Durability Tests

grafting method	polymer used	molecular weight (g/mol)	CA (°)	CAH (°)	durability (h)
vapor-phase	chlorine-terminated PDMS	277	102.5 ± 1.0°	1.6 ± 0.2°	39
		4000	103.0 ± 0.2°	1.0 ± 0.1°	39
		15 400	104.0 ± 0.5°	2.9 ± 0.5°	8
liquid-phase	silicone oil	17 250	103.0 ± 1.0°	3.5 ± 0.3°	25

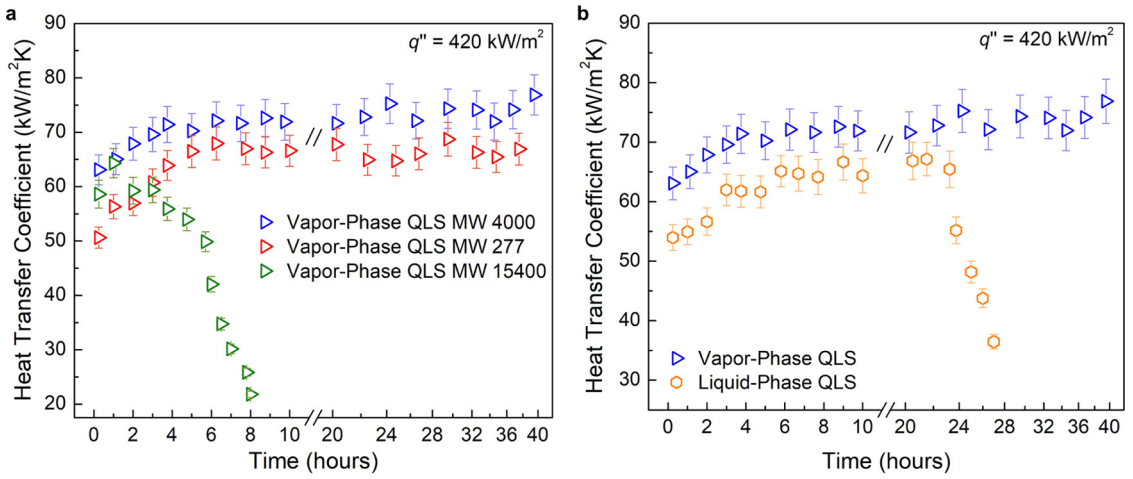

Figure 7. Sustainable high-performance dropwise condensation on the quasi-liquid surface under steam condensation. (a) Heat-transfer coefficient as a function of time for vapor-phase QLS. The oligomers have molecular weights of 277, 4000, and 15 400 g/mol. (b) Heat-transfer coefficient as a function of time for vapor-phase QLS and liquid-phase QLS. The heat flux of 420 kW/m^2 was maintained during durability tests for all of the samples.

We analyzed the water coverage ratio and droplet number density on these surfaces to quantitatively understand the influence of droplet dynamics on heat transfer. A small water coverage ratio shows faster condensate removal from the surface with a large refreshing area for condensation. Furthermore, the faster condensate removal leads to a higher density of small droplets (diameter <100 μm) due to rapid renucleation. Vapor-phase QLS has a water coverage ratio of 36%, while liquid-phase QLS and the silane surface have 130 and 150% higher water coverage ratios than that on the vapor-phase QLS, respectively (Figure 6a), because the higher CAH results in reduced droplet mobility. Moreover, the liquid-infused surface shows a 140% higher water coverage ratio compared to vapor-phase QLS due to the lubricant deletion at a large subcooling (Figure S10). Vapor-phase QLS has a high density of small droplets with diameters 10−70 μm due to the higher droplet removal frequency and surface refreshing for further nucleation. However, the liquid-phase QLS and silane surface have a higher density of large size droplets with diameters >280 μm (Figure 6b). The droplet departs at a smaller diameter on vapor-phase QLS than those on the liquid-phase QLS and silane surface. This is attributed to the ultralow CAH, which leads to faster shedding and a large density of small droplets (Movies S2 and S3). The small condensate droplets on the vapor-phase QLS reduced the thermal resistance for heat transfer. The ultralow CAH further improved surface refreshing with rapid droplet shedding. The vapor-phase QLS outperforms the liquid-phase QLS and silane

https://doi.org/10.1021/acsami.2c00401
ACS Appl. Mater. Interfaces 2022, 14, 13932−13941

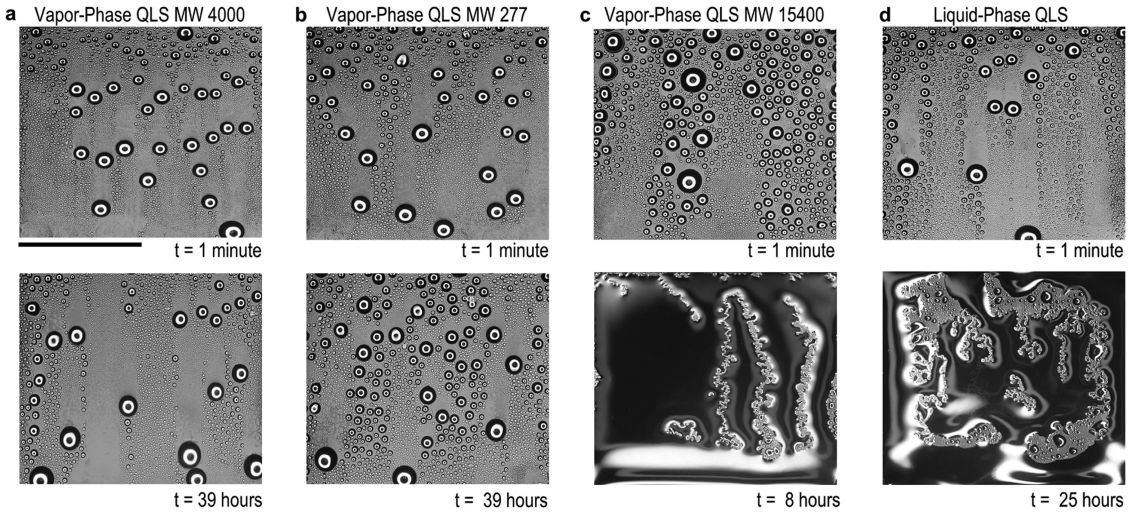

Figure 8. Visualization of continuous steam condensation on (a) vapor-phase QLS MW 4000, (b) vapor-phase QLS MW 277, (c) vapor-phase QLS MW 15 400, and (d) liquid-phase QLS. The scale bar is 1 cm.

surface in dropwise condensation of steam due to its ultralow CAH.

Optimization of Sustainable Steam Condensation. To demonstrate the potential impact of the QLS for steam condensation, we investigated the durability with two fabrication methods: vapor-phase and liquid-phase grafting. We used chlorine-terminated PDMS with three different molecular weights of 277, 4000, and 15 400 g/mol for surface fabrication using vapor-phase grafting, and the surfaces were named vapor-phase QLS MW 277, vapor-phase QLS MW 4000, and vapor-phase QLS MW 15 400, respectively. Liquid-phase QLS is grafted using silicone oil with a molecular weight of 17 250 g/mol. Silicone oils with different molecular weights were studied for the influence of molecular chain lengths and mobility.[46] The vapor-phase QLS fabricated using PDMS with a molecular weight of 4000 g/mol has the lowest CAH, while the vapor-phase QLS MW 277 and vapor-phase QLS MW 15 400 have higher CAH (Table 1). All of the durability experiments were performed in a closed chamber under pure steam with a pressure of 6.9 kPa above atmospheric pressure (Section S4 for details). During the steam condensation, a heat flux of 420 kW/m^2 was maintained 24 hours a day without a stop for all of the surfaces. Vapor-phase QLS MW 4000 and vapor-phase QLS MW 277 showed a sustained dropwise condensation under continuous steam generation for 39 h with a high heat-transfer coefficient of 71 kW/(m^2 K) (Figure 7a). However, the vapor-phase QLS MW 15 400 surface showed a reduced heat-transfer coefficient after 5 h due to the transition of dropwise condensation to filmwise condensation. Furthermore, the liquid-phase QLS surface showed a dropwise condensation with a sustained heat-transfer coefficient for 25 h. Once the coating degradation occurred, the heat-transfer coefficient was reduced to 33 kW/(m^2 K) with a partial film (Figure 7b).

Vapor-phase QLS MW 4000 and vapor-phase QLS MW 277 exhibited higher durability with stable dropwise condensation (Figure 8a,b). However, vapor-phase QLS MW 15 400 shows a filmwise condensation within 8 h (Figure 8c). The mechanism for the faster degradation of vapor-phase QLS MW 15 400 is attributed to the higher shear stress from the droplet shedding during steam condensation. The elongated chains may result in entanglement and restrict the mobility of molecular chains compared to those without entanglement.[45] The reduced chain mobility on vapor-phase QLS MW 15 400 provides a higher CAH of 2.9°, which imparts higher pinning compared to the lower CAH of 1 and 1.6° on vapor-phase QLS MW 4000 and MW 277, respectively. At the beginning of condensation (~1 min), liquid-phase QLS shows a dropwise mode. However, after 25 h of continuous condensation, the dropwise condensation transitions to partial filmwise condensation on liquid-phase QLS due to coating degradation (Figure 8d). The degradation of liquid-phase QLS with MW 17 250 g/mol is attributed to the elongated molecular chains that orient parallel to the surface, which could provide entanglement. This leads to reduced mobility of siloxane molecules and increases the CAH ($\Delta\theta$ = 3.5°). While QLS grafted using lower molecular weight 4000 g/mol has sufficiently flexible nonentangled molecular chains. The entanglement on liquid-phase QLS leads to higher pinning and increases the shear stress, which will degrade the liquid-phase QLS coating more easily.[46] The experimental investigation shows that the vapor-phase grafting with PDMS of molecular weights no more than 4000 can achieve smooth and homogenous coating with a sustained high-performance steam condensation.

CONCLUSIONS

We have shown that the condensation performance and sustainability on the QLS outperform those on SHS and SLIPS under steam condensation. The quasi-liquid surface showed a sustainable dropwise condensation due to the quasi-liquid interface, which consists of chemically bonded mobile molecule chains. We have studied steam condensation on the quasi-liquid surfaces made from vapor-phase and liquid-phase grafting, as well as the silane surface, respectively. The ultralow CAH on the vapor-phase QLS provides a rapid droplet removal due to the high departure speed and the reduced departure diameter of condensates. As a result, the vapor-phase QLS maintains a low percentage of the water coverage area that favors continual steam condensation. Consequently, dropwise condensation with high droplet mobility on the vapor-phase QLS shows up to 40, 70, and 380% heat-transfer enhancement compared to liquid-phase QLS, silane surface, and hydrophilic surface, respectively. The sustainable high-performance condensation heat transfer on

https://doi.org/10.1021/acsami.2c00401
ACS Appl. Mater. Interfaces 2022, 14, 13932−13941

the vapor-phase QLS directly validates the importance of ultralow CAH for condensation enhancement. This work demonstrates that the ultralow CAH leads to a large droplet departure speed and, in turn, minimizes the thermal resistance of condensed droplets. This sustains the heat-transfer performance and circumvents dropwise-to-filmwise condensation at elevated heat fluxes. The vapor-phase QLS shows a stable dropwise condensation with a high heat-transfer performance for a prolonged period of 39 h under day-and-night steam condensation. Our fundamental study of sustainable high-performance dropwise condensation on QLS will pave the way for a broad range of applications, including water harvesting, power generation, refrigeration and air conditioning, and thermal management.

METHODS

Fabrication of Quasi-Liquid Surfaces. Vapor-phase QLS was made by tethering the flexible polymer of chlorine-terminated poly(dimethylsiloxane) (Gelest Inc.) on a 2 cm × 2 cm silicon substrate with a one-step self-catalyzed grafting method. PDMS with three different molecular weights MW 277, MW 4000, and MW 15 400 was used. If not specified, the molecular weight 4000 PDMS was used to make the vapor-phase QLS in the entire work. The bare silicon substrates were treated with oxygen plasma to create a hydroxyl group and placed upside down on the cover of a Petri dish, which contained a 200 μL liquid chlorine-terminated PDMS oligomer. The assembly was placed in a vacuum oven (0.15 Torr, MTI Corporation EQ-DZF-6020-ETL) at 60 °C for 60 min. Sequentially, the substrates were rinsed in a toluene bath and placed inside the shaker for 2 min to ensure uniform rinsing and to clean untethered PDMS residues. Finally, the sample was cleaned with water and dried with nitrogen gas successively.

Liquid-phase QLS was made by tethering the flexible polymer of silicone oil (viscosity: 500 cSt from Gelest Inc.) on a silicon substrate with a one-step grafting method through immersion in the solvent mixture of silicone oil (Gelest Inc.) and *n*-heptane (99%, Sigma-Aldrich) in the ratio of 1:10. The substrates were immersed in the mixture for 48 h. The siloxane-grafted substrates with an excess silicone oil lubricant on the surface were immersed in a toluene bath inside the shaker for 2 min to remove the untethered lubricant layer from the surface.

Contact Angle Measurements. The contact angle measurements were carried out using a goniometer (Model 290, Rame-hart) at room temperature under ambient conditions (20−22 °C, ∼50% relative humidity). All of the contact angle values were averaged from 5 independent measurements by applying 5 μL droplets on the test surfaces. The contact angle hysteresis was measured by tilting the surface with respect to the horizontal plane until the droplet started to slide along the surface. Then, advancing, receding, and sliding angles of the droplets were measured by a computer program.

Steam Condensation Experiments. A custom-built steam chamber was used for the condensation tests. The system consists of a steam generator, a condensation chamber, a coolant unit, and a data acquisition system (Figure S6). The steam generator generates the steam at 100 °C, which is then supplied to the condensation chamber. A calibrated K-type thermocouple and a pressure gauge were installed to monitor the saturated working conditions (see Section S4 for details). The steam pressure was 6.9 kPa above atmospheric pressure and was maintained inside the chamber for the experiments. The percentage of noncondensable gases (NCGs) was calculated using Gibbs−Dalton's law, $\mathrm{NCG} = \frac{P_v - P_s(T_v)}{P_v} \times 100\%$, where P_v is the chamber pressure measured using the pressure gauge and $P_s(T_v)$ is the pressure that corresponds to the saturation temperature.[47] The temperature (T_v) measured by the thermocouple inside the chamber is 103 °C and the saturation vapor temperature corresponding to the steam pressure maintained in the chamber is 101.5 °C, which indicates that the steam is overheated for 1.5 °C. The calculated percentage of noncondensable gases is below 0%, which shows that it is steam condensation. The surfaces were mounted vertically in the condensation chamber and four thermocouples were installed on the condensing block to measure the temperature distribution. For the experiments, the temperature of circulating water was kept constant at 4 ± 0.2 °C using a chiller (NESLAB RTE-111) and the flow rate was varied to achieve the required subcooling. For visualization, a Nikon camera (D5600) was assembled with a macro lens (SIGMA 105 mm 1:2.8 DG MACRO HSM) to record the videos and images during steam condensation.

Characterization. Atomic force microscopy measurement was carried out in tapping mode using a Nanoscope V controller on a multimode microscope (Multimode IV, Bruker). The morphology of the samples was characterized by a scanning electron microscope (SEM, Supra-40, Zeiss).

ASSOCIATED CONTENT

Supporting Information

The Supporting Information is available free of charge at https://pubs.acs.org/doi/10.1021/acsami.2c00401.

Additional Figures S1−S10 and discussions regarding the materials, preparation of control surfaces, dropwise condensation on vapor-phase QLS-coated aluminum, experimental setup, data reduction, and the dropwise condensation model. Movies S1−S4 show the condensation on the durable quasi-liquid surface, which addresses the challenges of air and liquid lubricated surfaces, droplet dynamics on the quasi-liquid surfaces at a subcooling of 3 and 9 K, and the durability of quasi-liquid surfaces fabricated using vapor-phase and liquid-phase grafting (PDF)

Quasi-liquid surface addresses the durability challenges of air and liquid lubricated surfaces (MP4)

Condensed droplets are highly mobile on the vapor-phase QLS and depart rapidly from the surface (MP4)

With an increased subcooling, the droplet departure frequency further increases without flooding (MP4)

Condensation on the durable vapor-phase quasi-liquid surface (MP4)

AUTHOR INFORMATION

Corresponding Author

Xianming Dai − *Department of Mechanical Engineering, The University of Texas at Dallas, Richardson, Texas 75080, United States;* orcid.org/0000-0001-5050-2867; Email: Dai@utdallas.edu

Authors

Deepak Monga − *Department of Mechanical Engineering, The University of Texas at Dallas, Richardson, Texas 75080, United States*

Zongqi Guo − *Department of Mechanical Engineering, The University of Texas at Dallas, Richardson, Texas 75080, United States*

Li Shan − *Department of Mechanical Engineering, The University of Texas at Dallas, Richardson, Texas 75080, United States*

Seyed Adib Taba − *Department of Mechanical Engineering, The University of Texas at Dallas, Richardson, Texas 75080, United States*

Jyotirmoy Sarma − *Department of Mechanical Engineering, The University of Texas at Dallas, Richardson, Texas 75080, United States*

Complete contact information is available at:

https://doi.org/10.1021/acsami.2c00401
ACS Appl. Mater. Interfaces 2022, 14, 13932−13941

https://pubs.acs.org/10.1021/acsami.2c00401

Author Contributions

X.D. conceived and supervised the research. D.M. and X.D. designed the experiments. D.M. and L.S. carried out the experiments. D.M. and X.D. analyzed the data. D.M. and X.D. developed the heat-transfer model. D.M., Z.G., L.S., S.A.T., J.S., and X.D. wrote and revised the manuscript.

Notes

The authors declare the following competing financial interest(s): The authors declare that a United States provisional patent has been filed for this work.

■ ACKNOWLEDGMENTS

X.D., Z.G., and J.S. acknowledge the Young Investigator Program at Army Research Office (Award No. W911NF1910416). X.D. and D.M. acknowledge the National Science Foundation Faculty Early Career Development Program (Award No. 2044348), Early-Concept Grants for Exploratory Research (Award No. 1929677), and Major Research Instrumentation Program (Award No. 2018188). L.S. is supported by the startup funds at the University of Texas at Dallas (UT Dallas). S.A.T. is supported by the department teaching assistantship. This project is partially funded by the Office of Research at UT Dallas through the Core Facility Voucher Program.

■ REFERENCES

(1) Cho, H. J.; Preston, D. J.; Zhu, Y.; Wang, E. N. Nanoengineered Materials for Liquid−Vapour Phase-Change Heat Transfer. *Nat. Rev. Mater.* **2016**, *2*, No. 16092.

(2) Attinger, D.; Frankiewicz, C.; Betz, A. R.; Schutzius, T. M.; Ganguly, R.; Das, A.; Kim, C.-J.; Megaridis, C. M. Surface Engineering for Phase Change Heat Transfer: A Review. *MRS Energy Sustainability* **2014**, *1*, No. 4.

(3) Ma, J.; Sett, S.; Cha, H.; Yan, X.; Miljkovic, N. Recent Developments, Challenges, and Pathways to Stable Dropwise Condensation: A Perspective. *Appl. Phys. Lett.* **2020**, *116*, No. 260501.

(4) El Fil, B.; Kini, G.; Garimella, S. A Review of Dropwise Condensation: Theory, Modeling, Experiments, and Applications. *Int. J. Heat Mass Transfer* **2020**, *160*, No. 120172.

(5) Miljkovic, N.; Preston, D. J.; Enright, R.; Wang, E. N. Electric-Field-Enhanced Condensation on Superhydrophobic Nanostructured Surfaces. *ACS Nano* **2013**, *7*, 11043−11054.

(6) Gong, Z.; Su, Z.; Liu, X.; Pan, D.; Liu, J.; Zheng, H.; Joo, S. W. Boosting Electrically Actuated Manipulation of Water Droplets on Lubricated Surfaces through a Corona Discharge. *Langmuir* **2021**, *37*, 400−405.

(7) Oh, I.; Cha, H.; Chen, J.; Chavan, S.; Kong, H.; Miljkovic, N.; Hu, Y. Enhanced Condensation on Liquid-Infused Nanoporous Surfaces by Vibration-Assisted Droplet Sweeping. *ACS Nano* **2020**, *14*, 13367−13379.

(8) Holden, K.; Wanniarachchi, A.; Marto, P.; Boone, D.; Rose, J. The Use of Organic Coatings to Promote Dropwise Condensation of Steam. *J. Heat Transfer* **1987**, *109*, 768−774.

(9) Das, A.; Kilty, H.; Marto, P.; Andeen, G.; Kumar, A. The Use of an Organic Self-Assembled Monolayer Coating to Promote Dropwise Condensation of Steam on Horizontal Tubes. *J. Heat Transfer* **2000**, *122*, 278−286.

(10) Vemuri, S.; Kim, K.; Wood, B.; Govindaraju, S.; Bell, T. Long Term Testing for Dropwise Condensation Using Self-Assembled Monolayer Coatings of n-Octadecyl Mercaptan. *Appl. Therm. Eng.* **2006**, *26*, 421−429.

(11) Rausch, M.; Fröba, A.; Leipertz, A. Dropwise Condensation Heat Transfer on Ion Implanted Aluminum Surfaces. *Int. J. Heat Mass Transfer* **2008**, *51*, 1061−1070.

(12) Rausch, M. H.; Leipertz, A.; Fröba, A. P. On the Characteristics of Ion Implanted Metallic Surfaces Inducing Dropwise Condensation of Steam. *Langmuir* **2010**, *26*, 5971−5975.

(13) Paxson, A. T.; Yagüe, J. L.; Gleason, K. K.; Varanasi, K. K. Stable Dropwise Condensation for Enhancing Heat Transfer Via the Initiated Chemical Vapor Deposition (iCVD) of Grafted Polymer Films. *Adv. Mater.* **2014**, *26*, 418−423.

(14) Preston, D. J.; Mafra, D. L.; Miljkovic, N.; Kong, J.; Wang, E. N. Scalable Graphene Coatings for Enhanced Condensation Heat Transfer. *Nano Lett.* **2015**, *15*, 2902−2909.

(15) Miljkovic, N.; Enright, R.; Nam, Y.; Lopez, K.; Dou, N.; Sack, J.; Wang, E. N. Jumping-Droplet-Enhanced Condensation on Scalable Superhydrophobic Nanostructured Surfaces. *Nano Lett.* **2013**, *13*, 179−187.

(16) Anand, S.; Paxson, A. T.; Dhiman, R.; Smith, J. D.; Varanasi, K. K. Enhanced Condensation on Lubricant-Impregnated Nanotextured Surfaces. *ACS Nano* **2012**, *6*, 10122−10129.

(17) Wen, R.; Xu, S.; Ma, X.; Lee, Y.-C.; Yang, R. Three-Dimensional Superhydrophobic Nanowire Networks for Enhancing Condensation Heat Transfer. *Joule* **2018**, *2*, 269−279.

(18) Boreyko, J. B.; Chen, C.-H. Self-Propelled Dropwise Condensate on Superhydrophobic Surfaces. *Phys. Rev. Lett.* **2009**, *103*, No. 184501.

(19) Wen, R.; Li, Q.; Wu, J.; Wu, G.; Wang, W.; Chen, Y.; Ma, X.; Zhao, D.; Yang, R. Hydrophobic Copper Nanowires for Enhancing Condensation Heat Transfer. *Nano Energy* **2017**, *33*, 177−183.

(20) Ghosh, A.; Beaini, S.; Zhang, B. J.; Ganguly, R.; Megaridis, C. M. Enhancing Dropwise Condensation Through Bioinspired Wettability Patterning. *Langmuir* **2014**, *30*, 13103−13115.

(21) Hou, Y.; Yu, M.; Chen, X.; Wang, Z.; Yao, S. Recurrent Filmwise and Dropwise Condensation on a Beetle Mimetic Surface. *ACS Nano* **2015**, *9*, 71−81.

(22) Wang, H.; Nguyen, Q.; Kwon, J. W.; Ma, H. Condensation and Wetting Behavior on Hybrid Superhydrophobic and Superhydrophilic Copper Surfaces. *J. Heat Transfer* **2020**, *142*, No. 041601.

(23) Tokunaga, A.; Tsuruta, T. Enhancement of Condensation Heat Transfer on a Microstructured Surface with Wettability Gradient. *Int. J. Heat Mass Transfer* **2020**, *156*, No. 119839.

(24) Egab, K.; Alwazzan, M.; Peng, B.; Oudah, S. K.; Guo, Z.; Dai, X.; Khan, J.; Li, C. Enhancing Filmwise and Dropwise Condensation Using a Hybrid Wettability Contrast Mechanism: Circular Patterns. *Int. J. Heat Mass Transfer* **2020**, *154*, No. 119640.

(25) Wong, T.-S.; Kang, S. H.; Tang, S. K.; Smythe, E. J.; Hatton, B. D.; Grinthal, A.; Aizenberg, J. Bioinspired Self-Repairing Slippery Surfaces with Pressure-Stable Omniphobicity. *Nature* **2011**, *477*, 443−447.

(26) Lafuma, A.; Quéré, D. Slippery Pre-Suffused Surfaces. *Europhys. Lett.* **2011**, *96*, 56001−56005.

(27) Xiao, R.; Miljkovic, N.; Enright, R.; Wang, E. N. Immersion Condensation on Oil-Infused Heterogeneous Surfaces for Enhanced Heat Transfer. *Sci. Rep.* **2013**, *3*, No. 1988.

(28) Yao, Y.; Aizenberg, J.; Park, K.-C. Dropwise Condensation on Hydrophobic Bumps and Dimples. *Appl. Phys. Lett.* **2018**, *112*, No. 151605.

(29) Furmidge, C. Studies at Phase Interfaces. I. The Sliding of Liquid Drops on Solid Surfaces and A Theory for Spray Retention. *J. Colloid Sci.* **1962**, *17*, 309−324.

(30) Guo, Z.; Zhang, L.; Monga, D.; Stone, H. A.; Dai, X. Hydrophilic Slippery Surface Enabled Coarsening Effect for Rapid Water Harvesting. *Cell Rep. Phys. Sci.* **2021**, *2*, No. 100387.

(31) Dai, X.; Sun, N.; Nielsen, S. O.; Stogin, B. B.; Wang, J.; Yang, S.; Wong, T.-S. Hydrophilic Directional Slippery Rough Surfaces for Water Harvesting. *Sci. Adv.* **2018**, *4*, No. eaaq0919.

(32) Preston, D. J.; Lu, Z.; Song, Y.; Zhao, Y.; Wilke, K. L.; Antao, D. S.; Louis, M.; Wang, E. N. Heat Transfer Enhancement During Water and Hydrocarbon Condensation on Lubricant Infused Surfaces. *Sci. Rep.* **2018**, *8*, No. 540.

(33) Adera, S.; Alvarenga, J.; Shneidman, A. V.; Zhang, C. T.; Davitt, A.; Aizenberg, J. Depletion of Lubricant from Nanostructured Oil-

Infused Surfaces by Pendant Condensate Droplets. *ACS Nano* **2020**, *14*, 8024−8035.
(34) Seo, D.; Shim, J.; Lee, C.; Nam, Y. Brushed Lubricant-Impregnated Surfaces (BLIS) for Long-Lasting High Condensation Heat Transfer. *Sci. Rep.* **2020**, *10*, No. 2959.
(35) Wilke, K. L.; Antao, D. S.; Cruz, S.; Iwata, R.; Zhao, Y.; Leroy, A.; Preston, D. J.; Wang, E. N. Polymer Infused Porous Surfaces for Robust, Thermally Conductive, Self-Healing Coatings for Dropwise Condensation. *ACS Nano* **2020**, *14*, 14878−14886.
(36) Liu, P.; Zhang, H.; He, W.; Li, H.; Jiang, J.; Liu, M.; Sun, H.; He, M.; Cui, J.; Jiang, L.; Yao, X. Development of "Liquid-Like" Copolymer Nanocoatings for Reactive Oil-Repellent Surface. *ACS Nano* **2017**, *11*, 2248−2256.
(37) Yang, C.; Wu, Q.; Zhong, L.; Lyu, C.; He, G.; Yang, C.; Li, X.; Huang, X.; Hu, N.; Chen, M.; Hang, T.; Xie, X. Liquid-Like Polymer-Based Self-Cleaning Coating for Effective Prevention of Liquid Foods Contaminations. *J. Colloid Interface Sci.* **2021**, *589*, 327−335.
(38) Gao, P.; Wang, Y.; Wang, H.; Wang, J.; Men, X.; Zhang, Z.; Lu, Y. Liquid-Like Transparent and Flexible Coatings for Anti-Graffiti Applications. *Prog. Org. Coat.* **2021**, *161*, No. 106476.
(39) Zhang, L.; Guo, Z.; Sarma, J.; Dai, X. Passive Removal of Highly Wetting Liquids and Ice on Quasi-Liquid Surfaces. *ACS Appl. Mater. Interfaces* **2020**, *12*, 20084−20095.
(40) Schellenberger, F.; Xie, J.; Encinas, N.; Hardy, A.; Klapper, M.; Papadopoulos, P.; Butt, H.-J.; Vollmer, D. Direct Observation of Drops on Slippery Lubricant-Infused Surfaces. *Soft Matter* **2015**, *11*, 7617−7626.
(41) Park, K.-C.; Kim, P.; Grinthal, A.; He, N.; Fox, D.; Weaver, J. C.; Aizenberg, J. Condensation on Slippery Asymmetric Bumps. *Nature* **2016**, *531*, 78−82.
(42) Kreder, M. J.; Daniel, D.; Tetreault, A.; Cao, Z.; Lemaire, B.; Timonen, J. V.; Aizenberg, J. Film Dynamics and Lubricant Depletion by Droplets Moving on Lubricated Surfaces. *Phys. Rev. X.* **2018**, *8*, No. 031053.
(43) Wang, R.; Jakhar, K.; Ahmed, S.; Antao, D. S. Elucidating the Mechanism of Condensation-Mediated Degradation of Organofunctional Silane Self-Assembled Monolayer Coatings. *ACS Appl. Mater. Interfaces* **2021**, *13*, 34923−34934.
(44) Cha, H.; Vahabi, H.; Wu, A.; Chavan, S.; Kim, M.-K.; Sett, S.; Bosch, S. A.; Wang, W.; Kota, A. K.; Miljkovic, N. Dropwise Condensation on Solid Hydrophilic Surfaces. *Sci. Adv.* **2020**, *6*, No. eaax0746.
(45) Teisala, H.; Baumli, P.; Weber, S. A.; Vollmer, D.; Butt, H.-J. r. Grafting Silicone at Room Temperature—A Transparent, Scratch-Resistant Nonstick Molecular Coating. *Langmuir* **2020**, *36*, 4416−4431.
(46) Sarma, J.; Zhang, L.; Guo, Z.; Dai, X. Sustainable Icephobicity on Durable Quasi-Liquid Surface. *Chem. Eng. J.* **2022**, *431*, No. 133475.
(47) Alwazzan, M.; Egab, K.; Peng, B.; Khan, J.; Li, C. Condensation on Hybrid-Patterned Copper Tubes (I): Characterization of Condensation Heat Transfer. *Int. J. Heat Mass Transfer* **2017**, *112*, 991−1004.

https://doi.org/10.1021/acsami.2c00401
ACS Appl. Mater. Interfaces 2022, 14, 13932−13941